JMEPEG (2020) 29:4360–4369
https://doi.org/10.1007/s11665-020-04991-8

1059-9495/$19.00

Synergistic Effect of Grain Size, β-$Mg_{17}Al_{12}$, and Texture on Mechanical Properties of Mg-15Al (wt.%) Magnesium Alloy Processed by Equal Channel Angular Pressing

Yongpeng Zhuang, Hongxia Wang, Hang Li, Liuwei Zheng, Junjian Li, and Pengwen Zhou

(Submitted April 30, 2020; in revised form June 20, 2020; published online July 27, 2020)

In this study, the Mg-15Al (wt.%) alloy was processed via equal channel angular pressing technology through different passes. The effect of the grain size, β-$Mg_{17}Al_{12}$ particles and texture on the mechanical properties was systematically investigated. It is found that the grain size was significantly refined, and the reticular β-$Mg_{17}Al_{12}$ phase was broken into dispersed particles after multi-pass ECAP. A large amount of nanoscale $Mg_{17}Al_{12}$ particles also precipitate from α-Mg matrix. After 4-pass ECAP, the texture features a favorable alignment of the basal planes along 45° from the extrusion direction. In addition, the tensile strength and ductility are remarkably improved with increasing the extrusion pass and the best mechanical properties are achieved for the 4-pass ECAP (UTS = 269.3 MPa, EL = 8.1%), which can be ascribed to the grain boundary strengthening, the precipitation strengthening as well as the declined fragmentation effect of the reticular β-$Mg_{17}Al_{12}$ phase. However, under the ECAP conditions with large deformation, the yield strength shows a contrarily decreasing tendency. This is because the orientations of the basal poles in the texture present a nearly 45° to the extrusion axis proven by the higher Schmid factor (SF), making it much easier to start the sliding system of the Mg-15Al alloy during ECAP.

Keywords ECAP, high aluminum magnesium alloy, strengthening mechanism, texture

1. Introduction

Nowadays, Mg–Al alloys have become the most widely used commercial magnesium alloys (Ref 1-5). This is mainly attributed to the fact that the maximum solid solubility of Al element in Mg is 12.7%, while only 2.0% at room temperature. The Al element plays a role of refining grains as well as facilitating the precipitation of β-$Mg_{17}Al_{12}$ phase, and the strengthening effects increase with increasing the Al content (Ref 6). However, the hard and brittle β-$Mg_{17}Al_{12}$ phase will be connected into a network, while the Al content exceeds 9.0 wt.%, which breaks up the matrix and deteriorates the mechanical properties of Mg–Al alloy.

The ductility and strength are the main mechanical properties of any material but generally belong to the opposite features. Thus, materials may be ductile or strong, but they are rarely both (Ref 7, 8). Equal channel angular pressing (ECAP) technology is an effective means to refine the grain size and fragmentize the second-phase particles in the Mg–Al alloys (Ref 9), resulting in the improvement of strength and plasticity simultaneously (Ref 10, 11). Much research has obtained the Mg–Al alloys with excellent mechanical properties via ECAP process (Ref 12, 13). For example, the AZ61 with high yield strength of 205 MPa and elongation of 23.5% was prepared through ECAP by Jufu Jiang et al. (Ref 14). L.L. Tang et al. (Ref 15) obtained the AZ80 Mg alloy consisting of ultrafine-grained microstructure and nanoscale ellipsoidal-shaped particles, which is in favor of its outstanding properties (YS = 235 MPa, EL = 14.0%). The dispersed hard particles improve the strength through hindering the motion of dislocations and grain boundaries.

It was indicated that the deformation texture formed during ECAP process can also greatly influence the mechanical properties of Mg–Al alloys, since Mg alloy with HCP crystal lattice is sensitive to the crystallographic texture (Ref 16). It is usually considered that stronger texture after ECAP can improve the strength of Mg–Al alloy (Ref 17). In addition, the second-phase particles with larger size ($\geq$ 1 μm) influence the deformation texture due to the increased dislocation density and generation of a large deformation energy gradient in lattice defects, which also contributes to the strength increment (Ref 18, 19). However, some studies found that with increasing the ECAP pass, the tensile strength increases, while the yield strength obviously decreases for the AZ31 alloy (Ref 20, 21), which was ascribed to the formation of soften texture.

Therefore, in the past decades, many researches focus on improving the strength and plasticity of magnesium alloy with low aluminum content through ECAP via changing the grain size, the second-phase particle size and the texture. However, for Mg–Al alloys with high aluminum content (Al $>$ 9 wt.%), the reticular second-phase structure is the key to affect its mechanical properties, and it will significantly affect the formation of deformation texture, yet there are few studies on it. Hence, in the present study, Mg-15Al alloy with reticular structure was selected for multi-pass ECAP deformation. The effects of grain, reticular second phase and texture on the

Yongpeng Zhuang, Hongxia Wang, Hang Li, Liuwei Zheng, and **Junjian Li**, College of Materials Science and Engineering, Taiyuan University of Technology, Taiyuan, China; and **Pengwen Zhou**, Shanxi Aerospace Qinghua Equipment Co., Ltd, Changzhi, China. Contact e-mail: wanghxia1217@163.com.

mechanical properties of alloy were investigated systematically, and the corresponding mechanisms were discussed in detail.

2. Experimental Procedure

Commercially pure Mg and pure Al were used to prepare Mg-15Al (wt.%) alloy by heating to the temperature of 1043 k under protective gas atmosphere of SF_6 + CO_2 with the ratio of 99:1 in an induction resistance furnace. The melt was poured into a steel mold preheated to 473 k with a inner diameter of 88 mm. The chemical compositions of Mg-15Al alloy were measured using the inductively coupled plasma (ICP) spectrometer, as listed in Table 1. For ECAP experiment, the billets with the cross-section of 10 mm × 10 mm and the length of 100 mm were machined from the ingot. As-cast billets were not homogenized prior to ECAP. The lower the experimental temperature is, the easier it is to obtain fine grain. After ECAP at 543 K, there are shallow cracks on the surface layer, while at 553 K, the sample has no crack, so ECAP experiment was performed at 553 K using a tool steel die with an intersection angle of $\varphi = 110°$ and an outer arc of curvature of $\psi = 20°$. The specimens together with die were heated to 553 K and preserved for 15 min. Then, the samples were pressed at 0.04 mm/s for 1, 4 and 8 passes through route B_c.

The microstructure characterization was performed using an optical microscope ((LOM, Leica Microsystem GmbH, Wetzlar, German), a x-ray diffraction (XRD, Cu-Ka Dandong Ray instrument Co., Ltd., Dandong, China), a scanning electron microscope (SEM, TESCAN Ltd., Brno-Kohoutovice, Czech Republic) equipped with an electronic backscatter diffraction (EBSD, FEI Nova400, HKL-EBSD) and a transmission electron microscope (TEM, JEOL Ltd., Tokyo, Japan). The etching solution was a mixture of 4 vol.% HNO_3 and 96 vol.% alcohol. The samples for TEM analysis were prepared by Gatan691 ion milling. The sample speed is 4 rpm, the ion beam energy is 3.5 keV, and the angle of ion gun is ± 7°. The average grain size of the ECAPed samples and the uniform diameter of precipitate were calculated by the linear intercept method. Tensile testing was conducted on an universal testing machine (WDW-100KN) at room temperature and a constant tensile speed of 0.5 mm/min, and the gauge dimension of the tensile sample is 2 mm × 4 mm × 18 mm. At least three specimens were examined for each processing state.

3. Results and Discussion

3.1 Microstructure Development

The optical photograph of the as-cast Mg-15Al alloy is shown in Fig. 1(a). It is observed that the rose-like matrix about 70-100 μm is surrounded by the continuous network-shape second phase. The EDS results show that the rose-like phase is α-Mg matrix and the network-shape phase is eutectic β-$Mg_{17}Al_{12}$ phase, as shown in Fig. 1(c) and (d). The test points are indicated by arrows in Fig. 1(b).

Table 1 The chemical compositions of Mg-15Al

	Chemical compositions, wt.%						
Alloy	Al	Si	Cu	Ni	Fe	Be	Mg
Mg-15Al	14.6	0.19	0.21	0.07	0.12	0.05	Bal.

The microstructures and grain size distributions of ECAPed Mg-15Al alloys are exhibited in Fig. 2. For all the ECAPed alloys, the grain size distribution exhibits a log-normal shape approximately. The average grain size of 1-pass ECAPed sample is 10.64 μm. Homogeneous and fine microstructure is formed after 4 passes, with an mean grain size of 3.97 μm, as shown in Fig. 2(c) and (d). It is observed that the grain size increases to 7.22 μm after 8 passes, and some grains even grow up to ~ 23 μm. No recrystallized grain is observed in 1-pass-processed sample, showing that the grain refinement mechanism is mainly the mechanical shearing in the early period of ECAP process. Besides, after 4-pass EACP, numerous subcrystals less than 1 um are formed, which indicates that the recrystallization behavior occurs due to the increasing strain. The combination effects of dynamic recrystallization and mechanical shearing lead to the remarkable grain refinement after 4 passes. The grain growth after 8 passes can be ascribed to two main reasons. Firstly, the nucleation possibility of new recrystallization grain decreases due to the reduced density of dislocations attributed to the faster dislocation annihilation rate during the further processing (Ref 9, 22). Secondly, the mobility of grain boundary is enhanced due to the extension of heat preservation time for the 8-pass ECAP. Consequently, it is easy for the tiny grains with a large number of dislocations to recover and grow.

Figure 3(a), (b) and (c) exhibits SEM micrographs of the ECAPed Mg-15Al alloys. For the 1-pass process, some reticular β-$Mg_{17}Al_{12}$ phase is fractured and elongated along the extrusion direction on account of shear effect, as shown in Fig. 3(a). However, most of the β phase remains interconnect and aggregate severely. After 4 passes, the β phase is broken into island-shape particles and the reticular structure can be hardly observed. In addition, a great many of dispersed nanoscale particles precipitate from the α-Mg matrix (Ref 23), marked by yellow arrows shown in Fig. 3(d). The TEM observation and SAD patterns of fine particles demonstrates that the precipitated phase is $Mg_{17}Al_{12}$, as shown in Fig. 3(e). This is because, after 4-pass ECAP, the dislocation density in the α-Mg increases rapidly due to the large plastic deformation of first three passes and the dislocation tangles, resulting in the formation of many subgrain boundaries (Ref 24). Thus the grains are obviously refined and the amount of the grain boundaries is greatly increased. These grain boundaries, subgrain boundaries and dislocation provide abundant nucleation sites for the precipitated $Mg_{17}Al_{12}$ phase. Otherwise, the precipitation is also related to the thermal duration. The longer the holding time, the more energy in the crystal, and the easier for the nucleation of β-$Mg_{17}Al_{12}$. After 8 passes of ECAP, the reticular β phase is fractured seriously and few particles are precipitated from the matrix, as shown in Fig. 3(c). From the TEM micrographs of 8 passes, a little dislocation is observed around the grain boundary, which indicated that the resistance of grain growth decreases resulting in the grain coarsening.

Figure 4(a) displays the XRD patterns of as-cast and ECAP-processed Mg-15Al alloys. It can be seen that the alloys mainly consist of α-Mg matrix and β-$Mg_{17}Al_{12}$ phase. The volume fraction of the α-Mg and β-$Mg_{17}Al_{12}$ phases in Mg–Al alloys

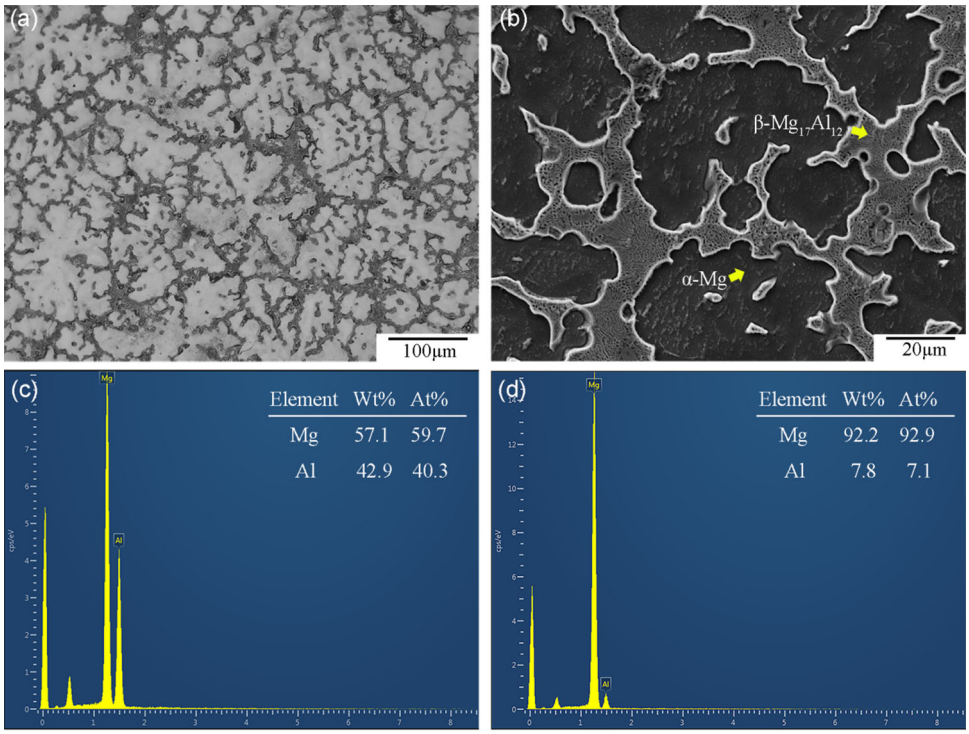

Fig. 1 (a) OM and (b) SEM micrographs with (c), (d) EDS spectra of as-cast sample

for different passes was quantitatively studied using the XRD K value method (Ref 25). We have:

$$w_\alpha = 1/(1 + K_\beta^\alpha I_\beta / I_\alpha) \quad \text{(Eq 1)}$$

$$v_\alpha = \frac{w_\alpha/\rho_\alpha}{w_\alpha/\rho_\alpha + w_\beta/\rho_\beta} \quad \text{(Eq 2)}$$

$$v_\alpha + v_\beta = 1 \quad \text{(Eq 3)}$$

where w_α is the weight fraction of α mixture, w_β is the weight fraction of β phase, $K_\beta^\alpha = K_\alpha/K_\beta$, K_α and K_β are constant, which depends upon the geometry of the diffractometer and the nature of component α and β, respectively, I_α intensity of x-rays diffracted by a selected plane (hkl) of component α, I_β intensity of x-rays diffracted by a selected plane (hkl) of component β, v_α the volume fraction of the α-Mg phase, ρ_α and ρ_β are the density of α phase and β phase, respectively. As for the Mg–Al alloy, K_α = 4.01, K_β = 2.41 (Ref 26), ρ_α = 1.738 g cm^{-3} and ρ_β = 2.1 g cm^{-3} (Ref 27). Thus the calculated results are shown in Fig. 4(b). It is not difficult to observe that the volume fraction of β-$Mg_{17}Al_{12}$ phase increases with increasing the ECAP pass number and a skip appears between 1 and 4 passes, which is in accordance with the precipitation of a large amount of nanoscale β phases (Fig. 3b).

3.2 Texture Development

It is generally known that texture type and strength (concentration degree) have significant effects on the properties of polycrystalline materials, especially for magnesium alloys with few slip systems. The pole diagrams of (0001) and (10-10) planes of ECAPed Mg-15Al alloys are depicted in Fig. 5. In the pole figures, the center of the coordinate is extrusion direction (ED), while X and Z are two directions perpendicular to ED. In 1-pass-processed samples (Fig. 5a), the maximum pole density is 10, and the areas with high pole density are mainly concentrated in the range of 38°-62° with the ED direction,; meanwhile, some areas with medium pole density appear at the two poles. Then, after 4 passes, the maximum pole density increased to 16.55, but the included angle between the area with high pole density and the extrusion axis decreased to 34°-56°, and no moderate pole density area appeared. Figure 5(b) clearly shows that the texture features the alignment of the basal planes along 45° away from ED. This texture was frequently observed in ECAPed Mg-based alloys (Ref 28, 29). During ECAP process, the rotation of basal planes is thought to be caused by shearing parallel to the basal planes (Ref 30). Eventually, after 8 passes of ECAP, it is noted that maximum density of (0001) pole diagram dropped to 7.17 heavily and the distribution range of angle between relatively high density area and extrusion axis narrowed to 44°-54°. However, more moderate density areas appear at two poles even other areas, which illustrates the formation of other oriented textures. The values of Schmid factor of Mg-15Al alloy with different states are calculated from the experimentally measured texture and are plotted in Fig. 6. It is found that the Schmid factor of 1-pass alloy is lower and the Schmid factor gradually increases with increasing the extrusion pass. Since a die with a channel angle of 110° is used in this investigation, the base plane of most grains is rearranged when the billet passes through the die. The base plane of magnesium alloy will be parallel to the extrusion direction or at an angle along the shear plane, featuring a higher Schmid factor, which is in favor of sliding of dislocation (Ref 31).

3.3 Mechanical Properties

The ultimate tensile strength (UTS), yield strength (YS) and elongation to fracture (EL) of the as-cast and the ECAP-

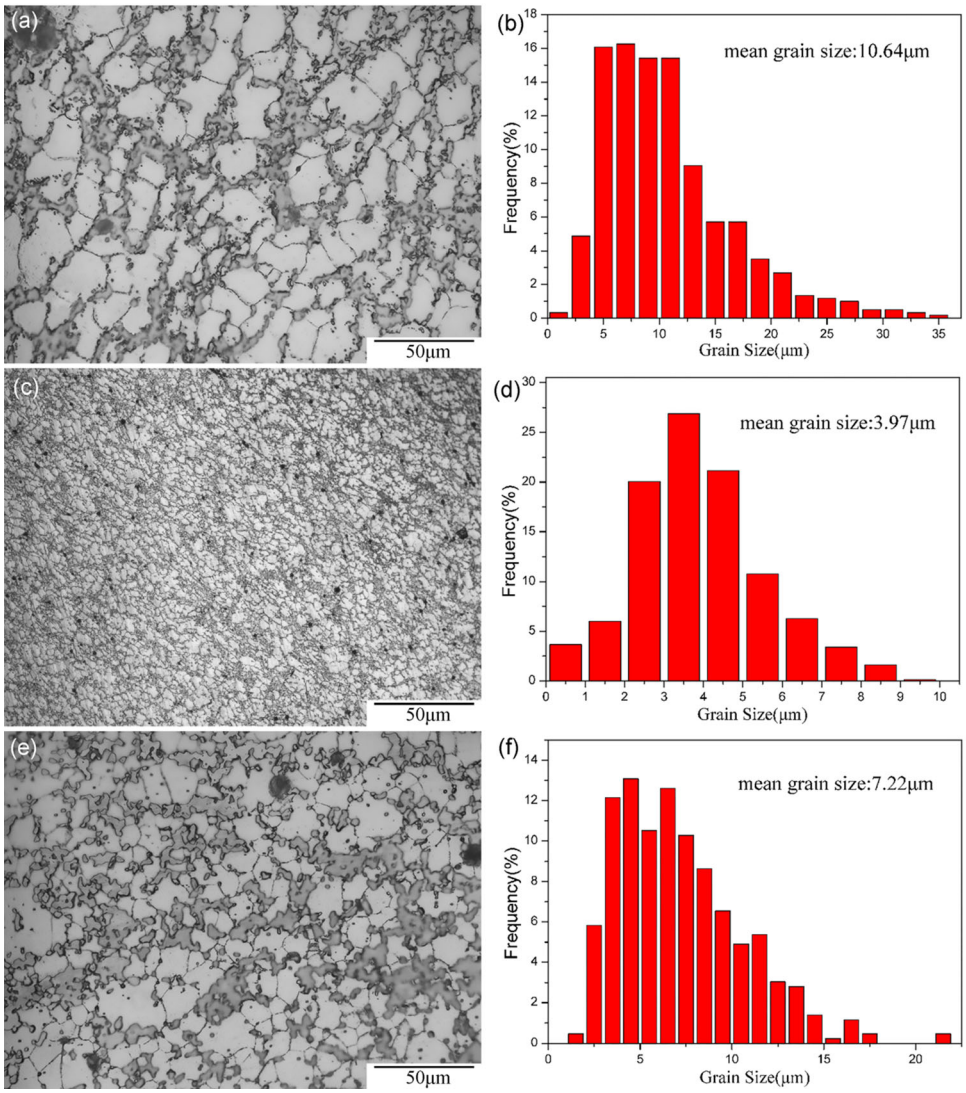

Fig. 2 Optical photographs and grain size distributions of the samples processed for different passes at 280°C: (a), (b) ECAP 1 pass, (c), (d) ECAP 4 passes, (e), (f) ECAP 8 passes

processed samples are exhibited in Fig. 7(a). Figure 7(b) displays the engineering stress–strain curves. It is found that after ECAP process, the UTS, YS and EL present a great rise. With increasing the extrusion pass, the UTS firstly increases and then decreases. This is because after ECAP process, the coarse grains were dramatically refined and the reticular β-$Mg_{17}Al_{12}$ phase was broken into small particles, which promotes the pinning effect of the grain boundary motion. Moreover, massive precipitation of nanoscale β-$Mg_{17}Al_{12}$ particles also contributes a lot to the UTS improvement via impeding dislocation motion. For the 8-pass ECAP process, the slight UTS decrease is mainly attributed to the grain coarsening because of the significant recovery and grain growth. The elongation of the as-cast alloy is 1.36%, which is on account of the coarse grains and the bulky reticular second phase cutting apart the α-Mg matrix. After the 4- and 8-pass ECAP, the Mg-15Al samples exhibit significantly increased elongation, which is 8.40% and 9.81%, respectively. There are two main reasons. Firstly, the finer microstructures reduce the stress concentration during the plastic deformation, which lowers the possibility of the crack generation. Secondly, the breakup of the reticular β-$Mg_{17}Al_{12}$ phase weakens the fragmentation effect to the α matrix.

It is worth noting that there is a sharp decline of the yield strength (YS) for the 4-pass ECAPed Mg-15Al alloys, which shows a great variation compared with the UTS. Similar phenomenon of the strength variation for the ECAPed Mg–Al alloys has been reported by other researches (Ref 31-33). It was mainly attributed to the softening caused by texture. Hence, the significant factors affecting the mechanical properties of ECAPed Mg-15Al is rather complicated, including the grain size, and size, morphology of the second phase as well as texture.

The strengthening mechanisms of the magnesium alloys processed by ECAP mainly contain grain boundary strengthening (σ_{HP}), precipitation strengthening (σ_{Or}).

According to the well-known Hall–Petch theory, σ_{HP} has to be calculated by the following equation (Ref 34, 35):

$$\sigma_{HP} = k\, d^{-\frac{1}{2}} \qquad \text{(Eq 4)}$$

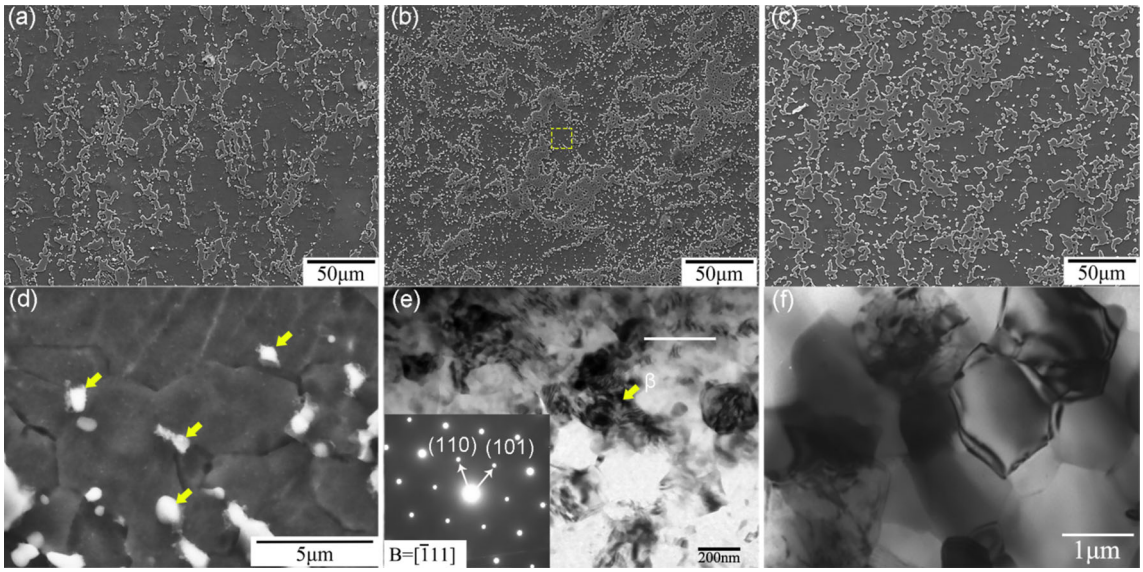

Fig. 3 SEM micrographs of (a) 1-pass, (b) 4-pass, (c) 8-pass ECAPed Mg-15Al alloys, (d) magnified SEM micrograph of 4-pass ECAPed sample, (e, f) TEM micrographs obtained from samples for 4 passes, 8 passes

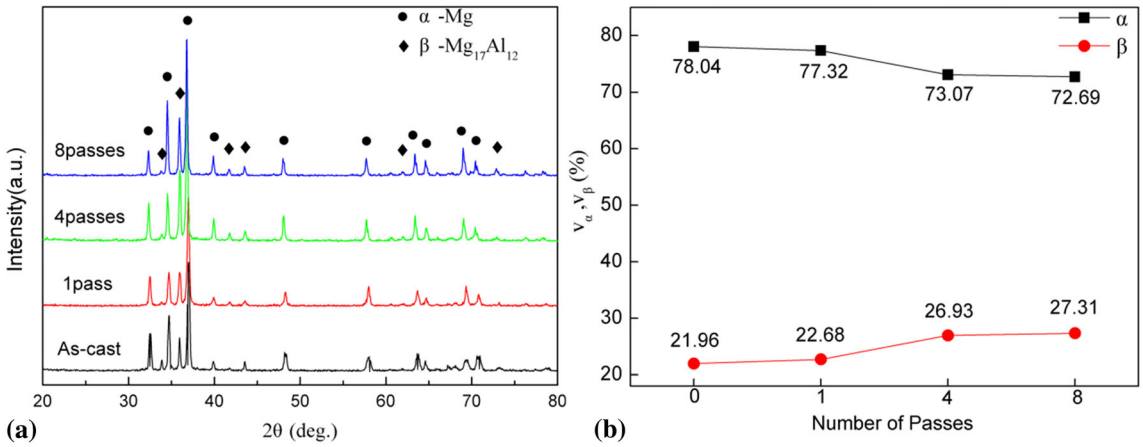

Fig. 4 (a) X-ray diffraction pattern of Mg-15Al alloy under different passes, (b) variation of volume fractions of α-Mg phase and β-$Mg_{17}Al_{12}$ phase with the number of passes

where k is the Hall–Petch slope and d is the average grain size. From Isaac Toda-Caraballo study, k value can be estimated by Ref 36:

$$k = k_{\mathrm{Mg}} + \sum_i X_i \Delta k_i \qquad \text{(Eq 5)}$$

where k_{Mg} = 0.21 (MPa $m^{0.5}$) is the strengthening coefficient of pure Mg, X_i the atomic solute content of element i and Δk_i is its variation on k. When i represents the Al element, Δk_i= 2 MPa $m^{0.5}at.^{-1}$ (Ref 36]. The k value is calculated by the content of elements in the second phase.

A lot of dynamically precipitated nanoscale β-$Mg_{17}Al_{12}$ particles distribute at the grain boundaries. The precipitation strengthening mechanism is assumed to be determined by the Orowan stress for bowing dislocations around the shear-resistant particles. Thus, the contribution to the YS can be calculated using the classical Orowan strengthening equation as follow (Ref 37):

$$\sigma_{\mathrm{Or}} = \frac{M G b}{2\pi\sqrt{1-\nu}} \frac{1}{\lambda} \ln \frac{d_p}{r_0} \qquad \text{(Eq 6)}$$

where M is Taylor factor taking value of the inverse of the measured Schmid factor, G is the shear modulus of Mg (G = 17.2GPa (Ref 38)), b is the Burgers vector (b = 0.32 nm (Ref 38)).d_p is the uniform diameter of precipitate, υ is Poisson ratio (υ = 0.35 (Ref 38)), r_0 is the inner cut-off radius of the dislocation taken equal to b (Ref 39), and λ is the effective planar inter-obstacle spacing. The dynamically precipitated particles can be regarded to be approximately spherical and λ can be calculated by the uniform diameter d_p of spherical particles, using equation (Ref 37).:

$$\lambda = \left(\frac{0.779}{\sqrt{f_p}} - 0.785 \right) \frac{d_p}{2} \qquad \text{(Eq 7)}$$

where f_p is the volume fraction of precipitates.

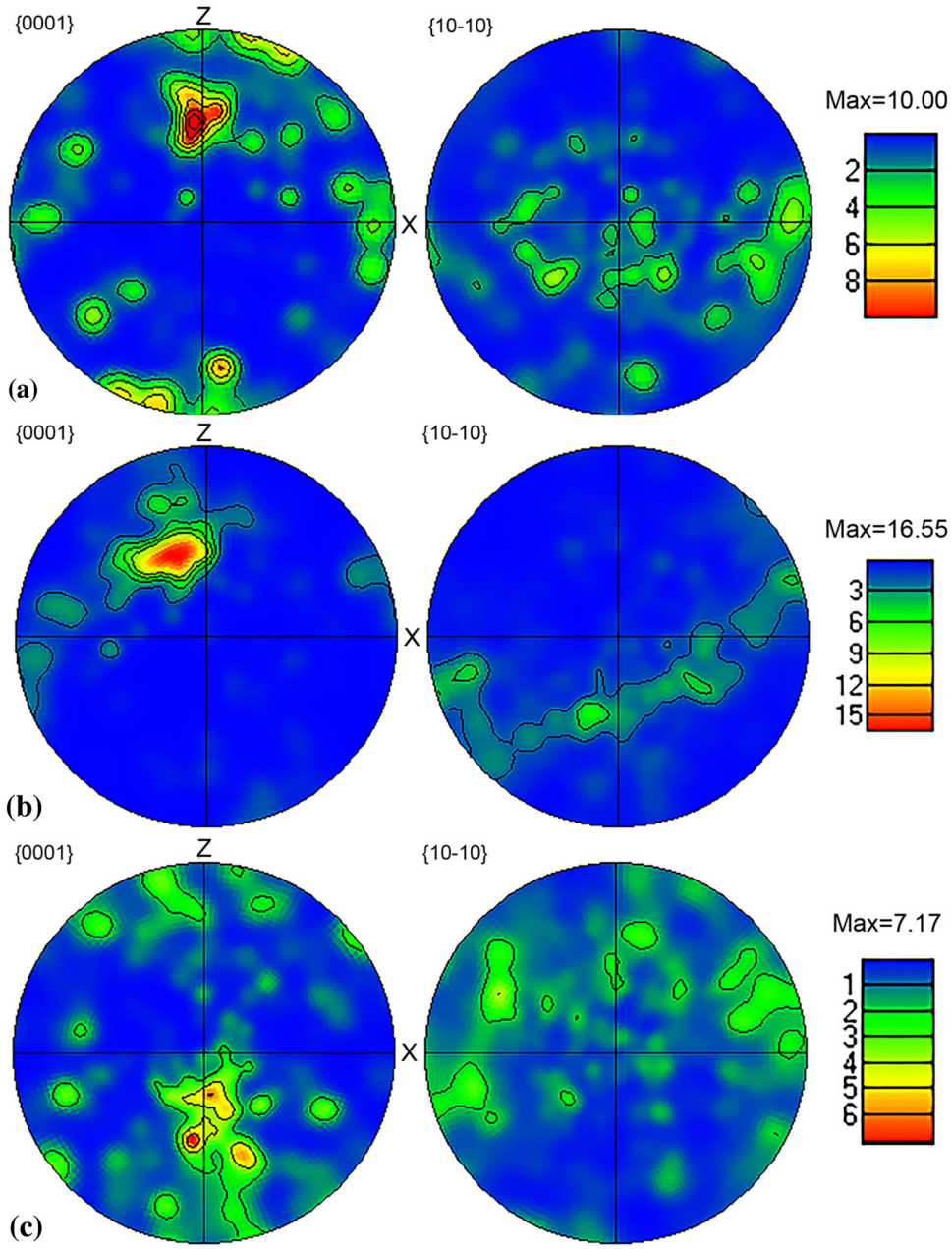

Fig. 5 The {0001} and {1010} pole figures of the ECAPed Mg-15Al alloy: (a) 1 pass, (b) 4 passes, (c) 8 passes

In this study, d_p and f_p were measured from the SEM and TEM images using the ImageJ software. For good statistics, at least 15 images from different locations were measured for each processing state and then the mean value was obtained. The measured results are shown in Table 2. Based on the above equation, the calculated strength values from grain boundary strengthening and Orowan strengthening are given in Table 2. Hence, the yield strength of ECAPed Mg-15Al alloys by summing the different strengthening results is obtained.

It can be seen that after 1-pass extrusion, the calculated sum value of two strengthening mechanisms is 132.1 MPa, which is close to the experimental result. This indicates that the grain refinement and precipitation strengthening play the dominant role in strength increment. For the 4- and 8-pass extruded samples, the calculated YS strength is 169.0 MPa and 114.9 MPa, respectively. However, the experimental strength values are much lower than the calculated results. The experimentally lower YS strength is mainly attributed to the negative effects of the texture formed during ECAP (Ref 13, 40, 41). During ECAP extrusion, the influence of texture on yield strength is expressed by the variation of Schmid factor of different slip systems. After 1-pass extrusion, the average Schmid factor is small, which indicates that most of the grains are in the hard orientation. Thus, the texture is not conducive to the beginning of the sliding system, while after 4 and 8 passes, the average Schmid factor increases gradually and thus the amount of grains in soft orientation increases a lot. The sliding occurs in most grains at the same time and easily propagates from one grain to the adjacent grain through the grain boundary. As the Schmid factor on (0 0 0 1) basal planes increases by the rotation of the basal poles to approximately 45° from the extrusion axis during ECAP, a lower stress for

yielding is needed on the basal plane for the ECAPed alloy (Ref 42, 43). Thus, it is easier for 4- and 8-pass-processed samples to reach the critical yield stress due to high SF, as shown in Fig. 5 and 6. As the softening effect caused by deformation texture is stronger than the mechanisms of grain refinement strengthening and precipitation strengthening, the yield strength is decreased after 4-pass ECAP (Ref 44, 45). Hence, the UTS of 4- and 8-pass ECAPed sample increases and the YS greatly decreases.

Figure 8 exhibits the SEM images of tensile fractures of the studied alloys. It can be observed that the fracture surface of as-cast alloy consists of several cracks (indicated by C), cleavage facets (indicated by A) and some residual second-phase particles (indicated by B), indicating a brittle cleavage fracture. After 1-pass ECAP, the area of cleavage facets and the number of cracks significantly reduce. Since the fracture surface is flat and the required energy for fracture is lower, the ductility of the alloy is still at a poor level. After 4-pass ECAP, some dimpled regions (indicated by D) appear on the fracture surface, presenting a ductile fracture (Ref 46), as shown in Fig. 8(c). For the 8-pass ECAP, the fracture morphology (Fig. 8d) is similar to that of 4-pass extrusion and the fracture mode is also ductile fracture. The observation results are in good agreement with the change of elongation. The longitudinal section images of Mg15Al alloys with different states show that many tensile microcracks were formed inside the β-$Mg_{17}Al_{12}$ phase, which indicates that the second phase are the origins of microcracks because of stress concentration between α-Mg matrix and them due to their high stiffness and brittleness (Ref 47, 48). For the 4-pass ECAP, the microcracks are hardly observed, because the grains and β phases are significantly broken resulting in relatively less stress concentration. Therefore, the 4-pass ECAPed alloy exhibits the best plasticity (Fig. 9).

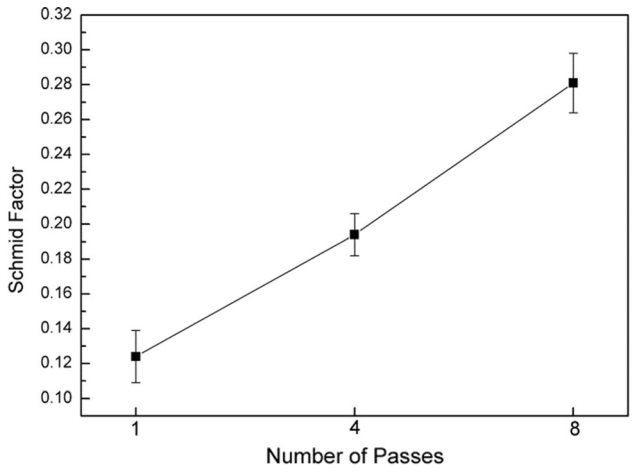

Fig. 6 The Schmid factors of Mg-15Al alloy with different states

4. Conclusions

In this study, the Mg-15Al alloy was processed via equal channel angular pressing (ECAP) technology at 553 K through different passes. The influence of grain size, precipitation and texture on mechanical properties of Mg-15Al alloy was systematically explored. The main conclusions can be drawn as follows:

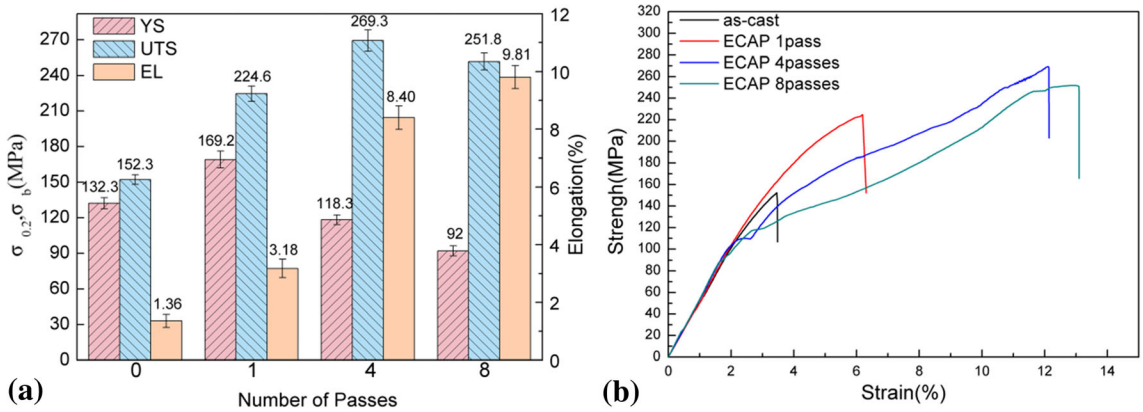

Fig. 7 (a) The relationship between strength and elongation and ECAP pass number at room temperature, (b)tensile stress and strain curves of the as-cast and ECAPed Mg-15Al alloys at room temperature

Table 2 The parameters and the calculation results

Pass time	m	k, MPa·lm$^{0.5}$	f_p, %	d_p, μm	σ_{HP}, MPa	σ_{Or}, MPa	Sum value, MPa
As-cast	…	304.2	…	…	33.0	0	33.0
1-pass	0.124	296.6	1.3	0.52	90.9	41.2	132.1
4-pass	0.194	248.8	3.4	0.55	124.9	44.1	169.0
8-pass	0.281	248	3.3	0.76	92.3	22.6	114.9

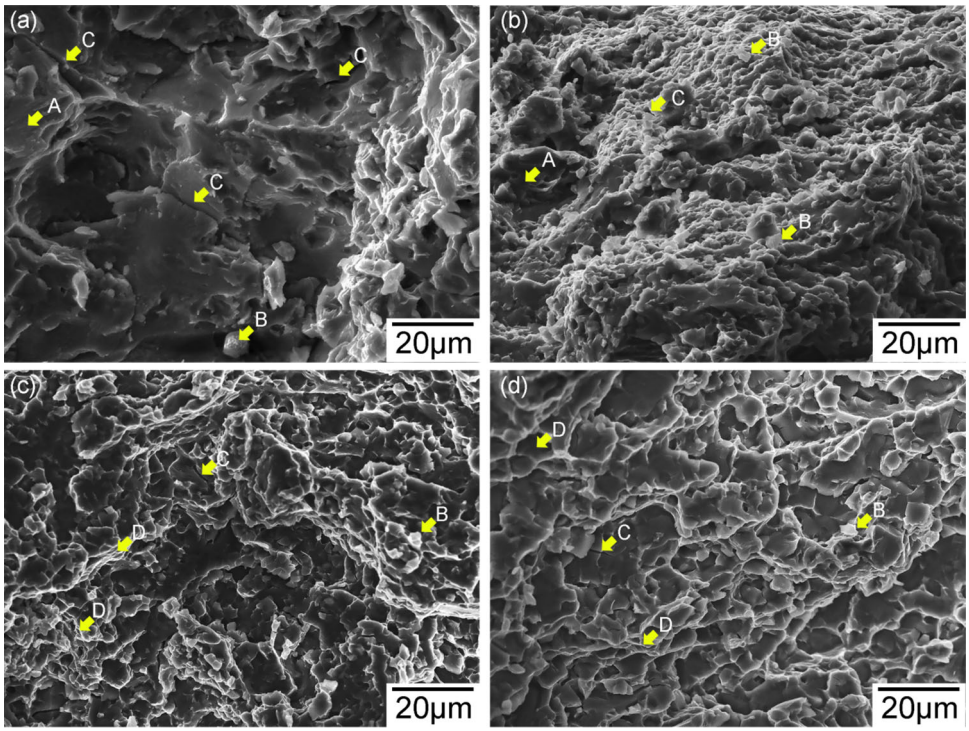

Fig. 8 SEM fracture morphology of the as-cast and ECAPed Mg15Al alloy after tensile test at room temperature: (a) as-cast, (b) 1 pass, (c) 4 passes, (d) 8 passes

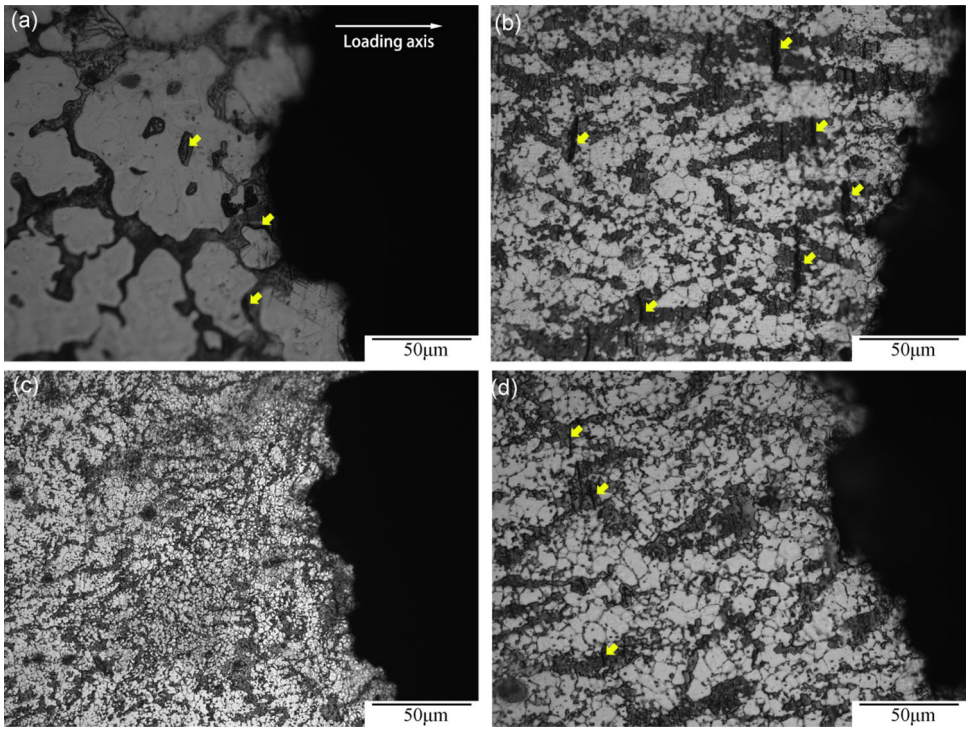

Fig. 9 Longitudinal of the fractured specimens of Mg-15Al alloys with different states: (a) as-cast, (b) 1 pass, (c) 4 passes, (d) 8 passes

1. ECAP processing has a remarkable refining effect on the grain of Mg-15Al alloy. With increasing the extrusion pass, the grain size decreases greatly. In addition, the reticular β phase is broken into island-shape particles, and numerous nanoscale $Mg_{17}Al_{12}$ particles precipitate from the α-Mg matrix after multi-pass ECAP.
2. After ECAP process, the fiber textures whose base orientation of [0001] was concentrated in the ED–Z plane and deviated from ED about 45° were formed. Meanwhile,

the Schmid factor gradually increases with the increasing extrusion pass.

3. With increasing the extrusion pass, the UTS of the Mg-15Al alloy firstly increases and then decreases, and the elongation greatly increases. The 4-pass ECAPed specimen shows the best mechanical property with UTS of 269.3 MPa and elongation of 7.4%. This is due to the grain boundary strengthening, the precipitation strengthening as well as the declined fragmentation effect of reticular β-$Mg_{17}Al_{12}$ phase.
4. With increasing the extrusion pass, the yield strength of the Mg-15Al alloy firstly increases slightly and then decreases remarkably, which is due to the softening of the α-Mg matrix caused by the texture variation that the orientations of the basal poles are nearly 45° to the extrusion axis. This can be proven by the higher Schmid factor (SF) for the multi-pass ECAP condition.

Acknowledgments

This work was supported by National Natural Science Foundation of China (51404166, 51704209, U1810208), Shanxi province scientific facilities and instruments shared service platform of magnesium-based materials electric impulse aided forming (201805D141005), Science and Technology Major Project of Shanxi province (20191102008, 20191102007, 20181101008), Natural Science Foundation of Shanxi Province (201701D121045), Patent Promotion and Implementation in Shanxi Province (20200718), and the Projects of International Cooperation in Shanxi (201803D421086).

References

1. E. Aghion, B. Bronfin, and D. Eliezer, The Role of the Magnesium Industry in Protecting the Environment, *J. Mater. Process. Technol.*, 2001, **117**, p 381 (in English)
2. R.Y. Lapovok, M. Barnett, and C.H. Davies, Construction of Extrusion Limit Diagram for AZ31 Magnesium Alloy by FE Simulation, *J. Mater. Process. Technol.*, 2004, **146**, p 408–414 ((in English))
3. N. Tahreen, D.L. Chen, M. Nouri, and D.Y. Li, Effects of Aluminum Content and Strain Rate on Strain Hardening Behavior of Cast Magnesium Alloys During Compression, *Mater. Sci. Eng. A*, 2014, **594**, p 235 ((in English))
4. Z.R. Zeng, Y.M. Zhu, R.L. Liu, S.W. Xu, C.H.J. Davies, J.F. Nie, and N. Birbilis, Achieving Exceptionally High Strength in Mg–3Al–1Zn–0.3Mn Extrusions via Suppressing Intergranular Deformation, *Acta Mater.*, 2018, **160**, p 97 ((in English))
5. T. Przemysław Snopiński, K. Tański, and S.Rusz Matus, Microstructure, Grain Refinement and Hardness of Al–3%Mg Aluminum Alloy Processed by ECAP with Helical Die, *Arch. Civ. Mech. Eng.*, 2019, **19**, p 287 ((in English))
6. A.K. Dahle, Y.C. Lee, M.D. Nave, P.L. Schaffer, and D.H. StJohn, Development of the As-Cast Microstructure in Magnesium-Aluminum Alloy, *J. Light Met.*, 2001, **1**, p 61 ((in English))
7. R.Z. Valiev and T.G. Langdon, Principles of Equal-Channel Angular Pressing as a Processing Tool for Grain Refinement, *Prog. Mater Sci.*, 2006, **51**, p 881 ((in English))
8. E. Damavandi, S. Nourouzi, S.M. Rabiee, and R. Jamaati, Effect of ECAP on Microstructure and Tensile Properties of A390 Aluminum Alloy, *Trans. Nonferrous Met. Soc. China*, 2019, **29**, p 931 ((in English))
9. M. Furukawa, Z. Horita, M. Nemoto, and T.G. Langdon, Review, Processing of Metals by Equal-Channel Angular Pressing, *J. Mater. Sci.*, 2001, **36**, p 2835 ((in English))
10. V.M. Segal, Materials Processing by Simple Shear, *Mater. Sci. Eng. A*, 1995, **197**, p 157 ((in English))
11. N.S. Martynenko, E.A. Lukyanova, V.N. Serebryany, M.V. Gorshenkov, I.V. Shchetinin, G.I. Raab, S.V. Dobatkin, and Y. Estrin, Increasing Strength and Ductility of Magnesium Alloy WE43 by Equal Channel Angular Pressing, *Mater. Sci. Eng. A*, 2018, **712**, p 625 ((in English))
12. K. Máthis, M. Köver, and J. Stráská, Micro-Tensile Behavior of Mg-Al-Zn Alloy Processed by Equal Channel Angular Pressing (ECAP), *Materials*, 2018, **11**, p 1644 ((in English))
13. X. Zhang and Y. Cheng, Tensile Anisotropy of AZ91 Magnesium Alloy by Equal Channel Angular Processing, *J. Alloys Compd.*, 2015, **622**, p 1105 ((in English))
14. J. Jiang, Y. Wang, and Q. Jianjun, Microstructure and Mechanical Properties of AZ61 Alloys with Large Cross-Sectional Size Fabricated by Multi-pass ECAP, *Mater. Sci. Eng., A*, 2013, **560**, p 473 ((in English))
15. L. Tang and R.K.Islamgaliev YonghaoZhao, Enhanced Strength and Ductility of AZ80 Mg Alloys by Spray Forming and ECAP, *Mater. Sci. Eng. A*, 2016, **670**, p 280 ((in English))
16. K.L. Murty and I. Charit, Texture Development and Anisotropic Deformation of Zircaloys, *Prog. Nucl. Energy*, 2006, **48**, p 325 ((in English))
17. L. Jin, D. Lin, and D. Mao, An Electron Back-Scattered Diffraction Study on the Microstructure Evolution of AZ31 Mg Alloy During Equal Channel Angular Extrusion, *J. Alloys Compd.*, 2006, **426**, p 148 ((in English))
18. R.D. Doherty, A.D. Rollett, D.A. Hughes, F.J. Humphreys, J.J. Jonas, D.J.Ô.K. Jensen, W.E. King, T.R. McNelley, and H.J. McQueen, Current Issues in Recrystallization: A Review, *Mater. Sci. Eng. A*, 1997, **238**, p 219 ((in English))
19. M. Hradilová, F. Montheillet, A. Fraczkiewicz, C. Desrayaud, and P. Lejček, Effect of Ca-Addition on Dynamic Recrystallization of Mg–Zn Alloy During Hot Deformation, *Mater. Sci. Eng., A*, 2013, **580**, p 217 ((in English))
20. K. Xia, J.T. Wang, X. Wu, G. Chen, and M. Gurvan, Equal Channel Angular Pressing of Magnesium Alloy AZ31, *Mater. Sci. Eng. A*, 2005, **410**, p 324 ((in English))
21. S.X. Ding, W.T. Lee, C.P. Chang, L.W. Chang, and P.W. Kao, Improvement of Strength of Magnesium Alloy Processed by Equal Channel Angular Extrusion, *Scr. Mater.*, 2008, **59**, p 1006 ((in English))
22. A. Heczel, F. Akbaripanah, M.A. Salevati, R. Mahmudi, Á. Vida, and J. Gubicza, A Comparative Study on the Microstructural Evolution in AM60 Alloy Processed by ECAP and MDF, *J. Alloys Compd*, 2018, **763**, p 629 ((in English))
23. C. Wang, A. Ma, J. Sun, H. Liu, H. Huang, Z. Yang, and J. Jiang, Effect of ECAP Process on As-Cast and As-Homogenized Mg-Al-Ca-Mn Alloys with Different Mg_2Ca Morphologies, *J. Alloys Compd.*, 2019, **793**, p 259 ((in English))
24. F. Guo, D. Zhang, and X. Yang, Strain-Induced Dynamic Precipitation of Mg17Al12 Phases in Mg–8Al Alloys Sheets Rolled at 748K, *Mater. Sci. Eng. A*, 2015, **636**, p 516 ((in English))
25. F.H. Chung, Quantitative Interpretation of X-Ray Diffraction Patterns of Mixtures III. Simultaneous Determination of a Reference Intensities, *J. Appl. Crystallogr.*, 1974, **7**, p 519 ((in English))
26. Yu Zhou, *Material Analysis Method*, 3rd ed., China Machine Press, Beijing, 2000, p 49–52 ((in Chinese))
27. Z.X. Feng, F.S. Pan, X.Y. Zhang, A.T. Tang, and Q.T. Fu, Distribution Characteristics of Mg17Al12 in Semi-Continuously Cast AZ61, *J. Mater. Eng.*, 2012, **2**, p 13 ((in English))
28. H. Huang, H. Liu, C. Wang, J. Sun, J. Bai, F. Xue, J. Jiang, and A. Ma, Potential of Multi-Pass ECAP on Improving the Mechanical Properties of a High-Calcium-Content Mg-Al-Ca-Mn Alloy, *J. Magn. Alloys*, 2019, **7**, p 617 ((in English))
29. X.G. Qiao, T. Ying, M.Y. Zheng, E.D. Wei, K. Wu, X.S. Hu, W.M. Gan, H.G. Brokmeier, and I.S. Golovin, Microstructure Evolution and Mechanical Properties of nano-SiCp/AZ91 Composite Processed by Extrusion and Equal Channel Angular Pressing (ECAP), *Mater. Charact.*, 2016, **121**, p 222 ((in English))
30. W.J. Kim, C.W. An, Y.S. Kim, and S.I. Hong, Mechanical Properties and Microstructures of an AZ61 Mg Alloy Produced by Equal Channel Angular Pressing, *Scr. Mater.*, 2002, **47**, p 39 ((in English))

31. W.J. Kim, S.I. Hong, Y.S. Kim, S.H. Min, H.T. Jeong, and J.D. Lee, Texture Development and Its Effect of Mechanical Properties of an AZ61 Mg Alloy Fabricated by Equal Channel Angular Pressing, *Acta Mater.*, 2003, **51**, p 3293 ((in English))
32. L. Jin, D.L. Lin, D.L. Mao, X.Q. Zeng, and W.J. Ding, Mechanic Properties and Microstructure of AZ3l Mg Alloy Processed by Two-Step Equal Channel Angular Extrusion, *Mater. Lett.*, 2005, **59**, p 2267 ((in English))
33. J.A. delValle, M.T. Perez-Prado, and O.A. Ruano, Texture Evolution During Large-Strain Hot Rolling of the Mg AZ61 alloy, *Mater. Sci. Eng. A*, 2003, **355**, p 68 ((in English))
34. E.O. Hall, The Deformation and Ageing of Mild Steel, *Proc. Phys. Soc. Sect. B*, 1951, **64**, p 747 ((in English))
35. N.J. Petch, The Cleavage Strength of Polycrystals, *J. Iron Steel Inst.*, 1953, **174**, p 25 ((in English))
36. I. Toda-Caraballo, E.I. Galindo-Nava, and Pedro E.J. Rivera-Diaz-del-Castillo, Understanding the factors influencing yield strength on Mg alloys, *Acta Mater.*, 2014, **75**, p 287 ((in English))
37. J.F. Nie, Effects of precipitate shape and orientation on dispersion strengthening in magnesium alloys, *Scr. Mater.*, 2003, **48**, p 1009 ((in English))
38. J.D. Robson and C. Paa-Rai, The interaction of grain refinement and ageing in magnesium-zinc-zirconium (ZK) alloys, *Acta Mater.*, 2015, **95**, p 10–19 ((in English))
39. C.R. Hutchinson, J.F. Nie, and S. Gorsse, Modeling the precipitation processes and strengthening mechanisms in a Mg-Al-(Zn) AZ91 alloy, *Metall. Mater. Trans. A*, 2005, **36**, p 2093 ((in English))
40. Yu Huihui, Y. Xin, Q. Liu, and M. Wang, Hall-Petch Relationship in Mg Alloys: A Review, *J. Mater. Sci. Technol.*, 2018, **34**, p 248 ((in English))
41. T. Krajňák, P. Minárik, J. Gubicza, K. Máthis, R. Kužel, and M. Janeček, Influence of Equal Channel Angular Pressing Routes on Texture, Microstructure and Mechanical Properties of Extruded AX41 Magnesium Alloy, *Mater. Charact.*, 2017, **123**, p 282 ((in English))
42. S.R. Agnew, J.A. Horton, T.M. Lillo, and D.W. Brown, Enhanced Ductility in Strongly Textured Magnesium Produced by Equal Channel Angular Processing, *Scr. Mater.*, 2004, **50**, p 377 ((in English))
43. D. Beining, H. Ziyang, J. Wang, L. Sheng, H. Zhao, Y. Zheng, and T. Xi, Effect of Extrusion Process on the Mechanical and In Vitro Degradation Performance of a Biomedical Mg-Zn-Y-Nd Alloy, *Bioact. Mater.*, 2020, **5**, p 219 ((in English))
44. R.D. Field, K.T. Hartwig, C.T. Necker, J.F. Bingert, and S.R. Agnew, Equal-Channel Angular Extrusion of Beryllium, *Metall. Mater. Trans. A*, 2002, **33**, p 965 ((in English))
45. G.G. Yapici and I. Karaman, Common Trends in Texture Evolution of Ultra-Fine Grained hcp Materials During Equal Channel Angular Extrusion, *Mater. Sci. Eng. A*, 2009, **503**, p 78 ((in English))
46. F. Bu, Q. Yang, K. Guan, X. Qiu, D. Zhang, W. Sun, T. Zheng, X. Cui, S. Sun, Z. Tang, X. Liu, and J. Meng, Study on the Mutual Effect of La and Gd on Microstructure and Mechanical Properties of Mg-Al-Zn Extruded Alloy, *J. Alloys Compd*, 2016, **688**, p 1241 ((in English))
47. B.N. Du, Z.P. Xiao, Y.X. Qiao, L. Zheng, B.Y. Yu, D.K. Xu, and L.Y. Sheng, Optimization of Microstructure and Mechanical Property of a Mg-Zn-Y-Nd Alloy by Extrusion Process, *J. Alloys Compd*, 2019, **775**, p 990 ((in English))
48. D. Bei-Ning, H. Zi-Yang, L.-Y. Sheng, X. Dao-Kui, Y.-F. Zheng, and T.-F. Xi, Influence of Zn Content on Microstructure and Tensile Properties of Mg–Zn–Y–Nd Alloy, *ACTA Metall Sin-Engl*, 2018, **31**, p 351 ((in English))